JOURNAL OF THE AMERICAN CHEMICAL SOCIETY

Communication

pubs.acs.org/JACS

In Situ CO_2-Emission Assisted Synthesis of Molybdenum Carbonitride Nanomaterial as Hydrogen Evolution Electrocatalyst

Yong Zhao, Kazuhide Kamiya, Kazuhito Hashimoto,* and Shuji Nakanishi*

Department of Applied Chemistry, The University of Tokyo, 7-3-1 Hongo, Bunkyo-ku, Tokyo 113-8656, Japan

Supporting Information

ABSTRACT: We reported a novel protocol to efficiently synthesize molybdenum carbonitride (MoCN) nanomaterials with dense active sites and high surface area. The key step in this protocol is the preparation of the catalyst precursor, which was obtained by polymerizing diaminopyridine in the presence of hydrogen carbonate. The abundant amino groups in the poly diaminopyridine bound numerous Mo species via coordination bonds, resulting in the formation of dense Mo active sites. The addition of hydrogen carbonate to the synthesis mixture resulted in CO_2 gas evolution as the local pH decreased during polymerization. The in situ evolved CO_2 bubbles mechanically broke down the precursor into MoCN nanomaterials with a high surface area. The synthesized MoCN materials were demonstrated as an electrocatalyst for hydrogen evolution reaction (HER). It exhibited an HER onset potential of −0.05 V (vs RHE) and a high hydrogen production rate (at −0.14 V vs RHE, −10 mA cm^{-2}) and is therefore one of the most efficient, low-cost HER catalysts reported to date.

Transition metal carbides (TMCs) and nitrides (TMNs), such as WC, MoC, MoN, etc., have attracted much attention since the first exhibition of their platinum-like behaviors for the catalytic formation of water from hydrogen and oxygen.[1] Consequently, TMCs/TMNs have been demonstrated as the efficient catalysts for a variety of chemical reactions, such as hydrogen evolution,[2−4] carbon dioxide (CO_2) reduction,[5] ammonia decomposition,[6] reformation,[7] water−gas shift,[8−10] and so on.[11−14] Compared to their parent metals, the higher catalytic activity of TMCs/TMNs originates from the introduction of heteroatoms, such as carbon, nitrogen, and other metals,[14−17] which influences the d-band electronic structure of parent metals, in turn optimizing the bond strengths between metal and absorbed reactive intermediates.[2,18,19]

Except for that, the catalytic activity of TMCs and TMNs are also highly influenced by the density of catalytic active sites (D_{cas}) and the effective surface area (S_{eff}). In general, TMCs and TMNs were obtained by direct carburization or ammonification of metal oxide/metal salt at high temperature.[6,17,20] D_{cas} of TMCs and TMNs are formed during long-term calcination; however, this process markedly decreases the S_{eff} due to aggregation of the crystallized materials.[16] To improve these two parameters, researchers have used several approaches. For example, Chen et al.[15] prepared a $NiMoN_x/C$ nanocatalyst by traditional nitridation of NiMo bimetals with ammonia gas and demonstrated that the imprinting of NiMo nanopowders on carbon nanoparticles markedly increased the S_{eff}. In addition, the pyrolysis of an aniline/molybdate hybrid precursor was used to synthesize Mo_2C nanowires without additional carbon support.[21] The D_{cas} in this Mo_2C material was higher than that of carbon particle-derived Mo_2C from the traditional carburization method because the C and Mo atoms were coordinated at the molecular level in the precursor. Although the S_{eff} or D_{cas} was independently enhanced step-by-step by these approaches, it remains a big challenge to largely increase both S_{eff} and D_{cas} simultaneously.

Here, we successfully developed a novel protocol to synthesize molybdenum carbonitride (MoCN) nanomaterials by using in situ CO_2 emission strategy and the abundant amino group-based polydiminopyridine precursors. Compared to the state-of-the-art MoC/MoN materials, the obtained MoCN materials showed much higher S_{eff} and D_{cas}. We characterized their activity by using electrocatalytic hydrogen evolution reaction (HER) as model system. It displayed highly efficient HER activities in acidic medium, which is the best among the family of TMCs and TMNs reported so far.

Our strategy for the synthesis of MoCN materials with both high S_{eff} and D_{cas} was divided into three synthetic steps (Scheme 1). In step 1, diluted hydrochloric acid was added to an aqueous solution of Na_2MoO_4 and diaminopyridine (DAP), forming a solid complex of DAP-$2H^+/MoO_4^{2-}$ (a). In step 2, a hybrid solution of $(NH_4)_2S_2O_8$ and $NaHCO_3$ was added to the suspension of (a) to produce polydiaminopyridine (PDAP)-$2H^+/MoO_4^{2-}$ (b).[22] $NaHCO_3$ was added for generating CO_2 gas bubbles in order to mechanically disrupt the solid-state monomer (a) and/or polymer (b), forming nanosized PDAP-$2H^+/MoO_4^{2-}$ complexes (b). It was speculated that the generation of large amounts of protons during the solid-phase polymerization of (a) would decrease the local pH, resulting in the evolution of CO_2 gas from $NaHCO_3$ via the following reaction: $HCO_3^- + H^+ \rightarrow CO_2 + H_2O$. It was confirmed that CO_2 gas bubbles were vigorously evolved during the polymerization reaction (Supplementary Movie 1) and that the particle size of PDAP-$2H^+/MoO_4^{2-}$ hybrid (b) was substantially decreased during this synthetic step (Figure S1). In the last step of the synthesis (step 3), polymer (b) was pyrolyzed at 800 °C to form MoCN nanomaterials.

As a starting material for the synthetic reaction, DAP monomer with two amino groups was selected because it enabled (i) the production of CO_2 gas during the polymerization

Received: November 13, 2014
Published: December 22, 2014

DOI: 10.1021/ja5114529
J. Am. Chem. Soc. 2015, 137, 110−113

Scheme 1[a]

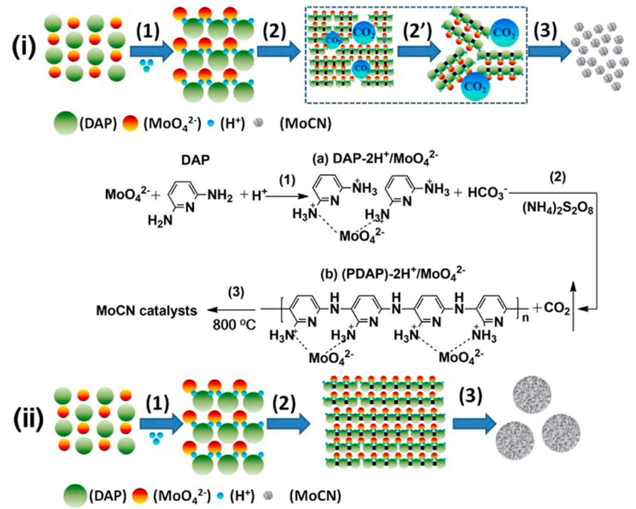

[a]Synthesis procedures of (i) PDAP-MoCN-CO_2 and (ii) PDAP-MoCN catalysts. (1) Coordination of DAP, proton, and molybdate; (2) polymerization of DAP-$2H^+/MoO_4^{2-}$ with $(NH_4)_2S_2O_8$ oxidant (2′, splitting PDAP-$2H^+/MoO_4^{2-}$ and/or DAP-$2H^+/MoO_4^{2-}$ complex to nanoparticles by in-situ CO_2-evolution); (3) pyrolysis of PDAP-$2H^+/MoO_4^{2-}$. DAP, diaminopyridine; PDAP, polydiaminopyridine.

reaction due to the formation of many protons and (ii) the coordination of MoO_4^{2-} ions with amino groups in the resultant PDAP polymer. The former and latter properties would be beneficial for obtaining high S_{eff} and D_{cas}, respectively. Hereafter, we called the resultant pyrolyzed product as PDAP-MoCN-CO_2. We also synthesized two other MoCN materials as reference samples. The first (termed PDAP-MoCN) was prepared without adding HCO_3^- during step 2, and the second (termed PANI-MoCN) was prepared using polyaniline (PANI), which has fewer amino groups than PDAP, as the polymer precursor.

We first examined the HER activities of PDAP-MoCN-CO_2, PDAP-MoCN, and PANI-MoCN in a sulfuric acid (H_2SO_4) solution (pH 1) using a rotating ring-disk electrode (RRDE) system (Figure 1a), and the rotation speed of RRDE was set to 1000 rpm to quickly remove H_2 gas from the disk electrode and to allow detection of the H_2 oxidation current at the Pt-ring electrode. The pyrolysis time was optimized to be 1 h at 800 °C (Figure S2). Commercial Pt/C (20 wt %) was used as the reference catalyst (curve 1). As shown in Figure 1a, PDAP-MoCN-CO_2 catalyst generated a cathodic current with an onset potential (U_{onset}) of −0.05 V and a potential of −0.14 V at −10 mA cm^{-2} (U_{-10}) (curve 2). When the Pt-ring electrode potential was set at +0.30 V, at which only the H_2 oxidation reaction can proceed, both anodic current and cathodic disc-current were detected (Figure 1b), indicating that the cathodic current is due to HER. The potential gap at U_{-10} between PDAP-MoCN-CO_2 and commercial Pt/C catalyst was only 60 mV, demonstrating that the PDAP-MoCN-CO_2 catalyst was highly active for HER. The catalytic HER current was stable, as has been reported for other MoC/MoN materials,[4] even after 1000 cycles of potential scan between −0.35 and 0.2 V (Figure S3).

Tafel slope is one of the indicators for the kinetic activity of electrodes, which is plotted in Figure S4.[23,24] Tafel slope of PDAP-MoCN-CO_2 was calculated to be 46 mV dec^{-1}, a little better than PDAP-MoCN (51 mV dec^{-1}) and PANI-MoCN catalysts (50 mV dec^{-1}). Tafel slope of the commercial Pt/C was around 36 mV dec^{-1}, which was better than that of MoCN materials. HER kinetic activity was strongly correlated with metal−H_{ads} bond strength, and the optimized strength can be evaluated from volcano plots.[19,25] The values of tafel slopes for MoCN electrodes, 46−51 mV dec^{-1}, suggested that the HER mechanism possibly occurred via a Volmer−Heyrovsky mechanism,[15,26] in which proton reacted with H_{ads} and the second electron to get H_2 gas as the limited step. The U_{onset} (−0.05 V) for PDAP-MoCN-CO_2 is one of the highest among the reported Mo- and W-based HER catalysts, including oxygen-incorporated MoS_2 nanosheet (approximately −0.15 V),[27] layered MoS_2 (approximately −0.15 V),[28] Mo_2C nanowires (approximately −0.08 V),[21] and Fe-WCN electrocatalysts (approximately −0.1 V).[2] The U_{-10} value (−0.14 V) is also one of the highest among Mo- and W-based materials reported to date (−0.17 V for oxygen-incorporated MoS_2 nanosheet,[27] −0.20 V for CoMoN,[29] −0.25 V for NiMoN_x/C nanosheets,[15] and −0.21 V for MoB particles[30]).

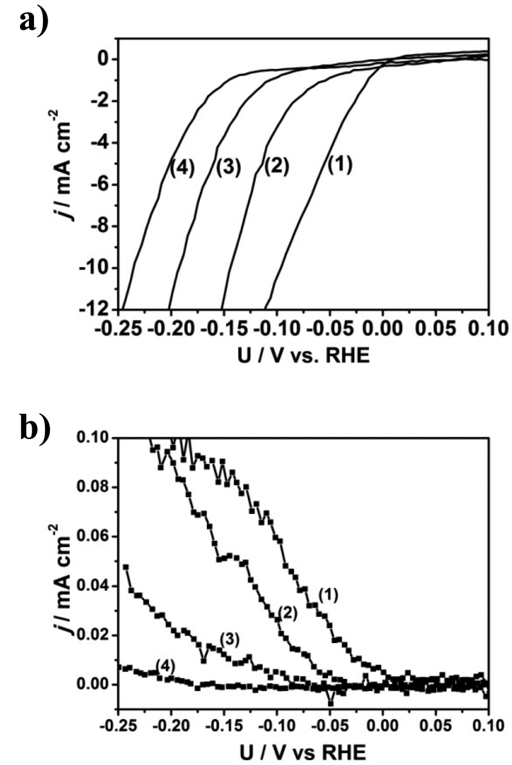

Figure 1. (a) HER polarization curves for (1) commercial Pt/C; (2) PDAP-MoCN-CO_2; (3) PDAP-MoCN; and (4) PANI-MoCN electrodes; (b) H_2 production detected at Pt ring electrode. Scan rate, 5 mV s^{-1}; rotational speed, 1000 rpm; catalyst loading, 0.4 mg cm^{-2}; geometrical surface area, 0.2 cm^2.

As shown in Figure 1a, the activity of PDAP-MoCN-CO_2 was markedly higher than that of PDAP-MoCN (curve 3, U_{onset} = −0.09 V, U_{-10} = −0.19 V) and PANI-MoCN catalysts (curve 4, U_{onset} = −0.12 V, U_{-10} = −0.23 V). The effect of in situ CO_2 gas evolution on S_{eff} was confirmed by comparing the morphologies of the PDAP-MoCN-CO_2 and PDAP-MoCN materials. From scanning electron microscopic (SEM) images, it was determined that PDAP-MoCN-CO_2 nanoparticles ranged in diameter from 20 to 30 nm and were uniformly distributed (Figure 2a,b). In contrast, the particle sizes of PDAP-MoCN were much larger, in the range of hundreds of nanometers (Figures 2c and S5). In agreement with the morphological differences in particle size, the Brunauer−Emmett−Teller (BET) specific surface area of

DOI: 10.1021/ja5114529
J. Am. Chem. Soc. 2015, 137, 110−113

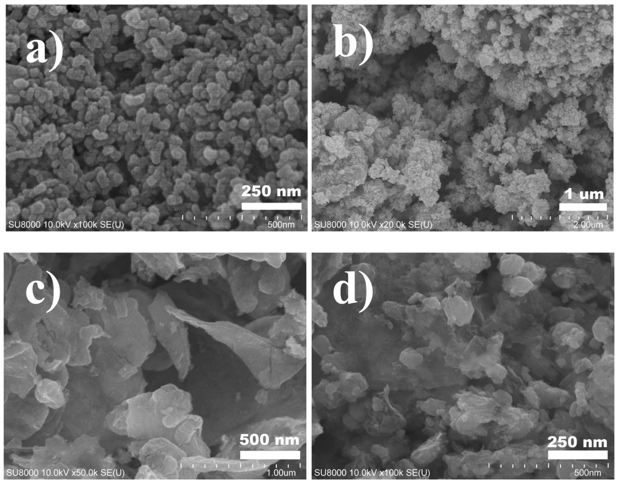

Figure 2. SEM images of (a,b) PDAP-MoCN-CO_2, (c) PDAP-MoCN, and (d) PANI-MoCN materials.

PDAP-MoCN-CO_2 (107 m^2 g^{-1}), as determined by low-temperature N_2 adsorption desorption isotherms, was much larger than that of PDAP-MoCN (6 m^2 g^{-1}) (Figure S6). The higher BET surface area of PDAP-MoCN-CO_2 was associated with a 4-fold greater electrochemically active surface area (EASA, Figure S7).

PDAP-MoCN-CO_2 was further analyzed by energy-dispersive spectroscopy (EDS−TEM (Figure 3), which revealed that the

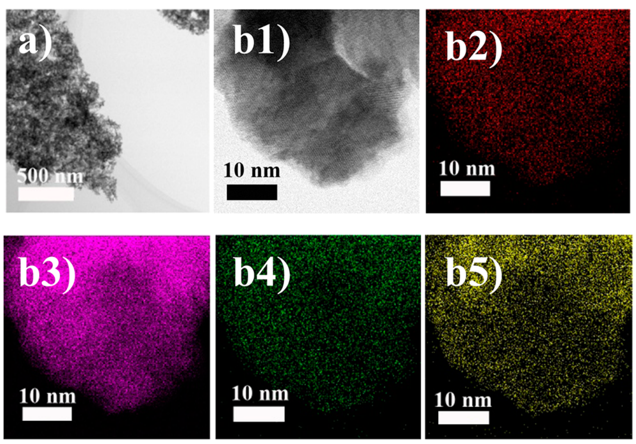

Figure 3. (a) TEM images and (b) EDS elemental mapping of PDAP-MoCN-CO_2 materials (b1, original; b2, C; b3, O; b4, N; and b5, Mo).

elements C, N, Mo, and O were uniformly distributed on the sample surface. The elemental contents of PDAP-MoCN-CO_2 and PDAP-MoCN were also characterized by X-ray photoelectron spectroscopy (XPS, Table 1), in which they exhibited very similar elemental compositions. As expected, these results indicated that in situ CO_2 gas evolution during the polymerization reaction effectively increased the S_{eff} through a decrease of the particle size, but did not change the elemental composition.

Table 1. Relative Elemental Contents of the MoCN Materials As Determined by XPS (the Bracket Values in the Mo Column Are the Total Concentrations of Mo^{2+} and Mo^{3+})

catalyst	C (mol %)	N (mol %)	O (mol %)	Mo (mol %)
PDAP-MoCN-CO_2	47.5	22.4	15.4	14.7 (12.8)
PDAP-MoCN	46.5	23.0	16.0	14.5 (12.6)
PANI-MoCN	53.5	18.8	19.5	8.2 (5.1)

The effect of the precursor material on D_{cas} was evaluated by comparing PDAP-MoCN and PANI-MoCN. Using SEM, the particle size of PANI-MoCN (Figures 2d) was shown to be much smaller than that of PDAP-MoCN (Figures 2c). The BET surface area of PANI-MoCN material was estimated to be approximately 55 m^2 g^{-1}, which is much larger than the value of 6 m^2 g^{-1} estimated for PDAP-MoCN. However, the HER activity of PANI-MoCN was lower than that of PADP-MoCN, despite the larger S_{eff} for PANI-MoCN (Figure 1a). We speculated that this difference in the HER activity was due to the much lower D_{cas} of PANI-MoCN (5%) in contrast to that of PDAP-MoCN (13%) materials, a hypothesis that is strongly supported by the results of the XPS surface elemental analyses. Figure 4 displays the Mo 3d

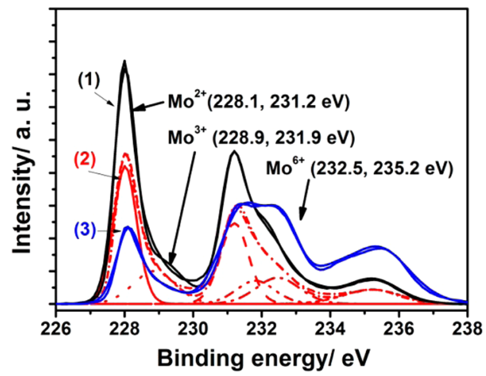

Figure 4. XPS Mo 3d spectra of (1) PDAP-MoCN-CO_2, (2) PDAP-MoCN, and (3) PANI-MoCN materials. (Both of the measured and simulated curves are presented.)

spectra of the MoCN materials, including PDAP-MoCN-CO_2. The Mo 3d spectra were deconvoluted into six peaks, assignable to Mo^{2+} (228.1 and 231.2 eV), Mo^{3+} (228.9 and 231.9 eV), and Mo^{6+} (232.5 and 235.2 eV) species.[13,31,32] Mo^{6+} is assigned to molybdenum oxides,[31] whereas Mo^{2+} and Mo^{3+} are thought to be molybdenum carbides and nitrides,[13,32] respectively, which are known to serve as active sites for HER.[15]

The total concentrations of Mo species in PDAP-MoCN and PDAP-MoCN-CO_2 exceeded 14 mol % (Table 1), which are much higher than that in PANI-MoCN (8 mol %). This larger difference is likely attributable to the 2-fold higher amount of amino groups in PDAP as compared to PANI, and to the higher capacity for N-coordinated MoO_4^{2-} species in the PDAP polymer matrix. In addition, the total amounts of Mo^{2+} and Mo^{3+} species (the bracket in Table 1) in PDAP-MoCN and PDAP-MoCN-CO_2 (over 13 mol %) are also much higher than that in PANI-MoCN (5 mol %). Mo^{2+} and Mo^{3+} represented nearly 90% of the total Mo species in PDAP-MoCN and PDAP-MoCN-CO_2. In contrast, the content of active Mo species in PANI-MoCN was only 60% of the total Mo species. Taken together, these findings show that the D_{cas} of PDAP-MoCN and PDAP-MoCN-CO_2 was more than 2-fold greater than that of PANI-MoCN.

To further confirm that Mo^{2+} and Mo^{3+} are the active species for HER, we oxidized the surface of PDAP-MoCN-CO_2 by scanning the potential up to 1.9 V. As shown in Figure S8, the HER activity was almost undetectable at the examined potentials after the electrochemical oxidation of catalyst surface. XPS analyses revealed that the Mo^{2+} and Mo^{3+} species were oxidized to Mo^{6+} by the surface oxidation process. This result strongly

DOI: 10.1021/ja5114529
J. Am. Chem. Soc. 2015, 137, 110−113

supported the finding that Mo carbide/nitride were responsible for the HER activity of MoCN materials.

In summary, we developed a novel protocol to fabricate MoCN nanomaterials that involves synthesizing Mo-rich PDAP-$2H^+/MoO_4^{2-}$ precursor and breaking down the microsized precursor to nanoparticles with the assistance of in situ CO_2 emission. The resultant catalytic materials had high specific surface area and dense active sites and exhibited high HER activities. We anticipate that various functional materials can be synthesized using the novel protocol developed here, as the synthesis strategy is applicable to the carbonitrides of other early transition metals, such as W, Nb, and Ta.

■ ASSOCIATED CONTENT

Ⓢ Supporting Information

Experimental procedures, precursor morphology, optimized synthesis condition, HER stability, BET surface area, EASA, Tafel plots, and electrochemical oxidation of electrode. This material is available free of charge via the Internet at http://pubs.acs.org.

■ AUTHOR INFORMATION

Corresponding Authors

*hashimoto@light.t.u-tokyo.ac.jp
*nakanishi@light.t.u-tokyo.ac.jp

Notes

The authors declare no competing financial interest.

■ REFERENCES

(1) Levy, R. B.; Boudart, M. *Science* **1973**, *181*, 547.
(2) Zhao, Y.; Kamiya, K.; Hashimoto, K.; Nakanishi, S. *Angew. Chem., Int. Ed.* **2013**, *52*, 13638.
(3) Chen, W. F.; Wang, C. H.; Sasaki, K.; Marinkovic, N.; Xu, W.; Muckerman, J. T.; Zhu, Y.; Adzic, R. R. *Energy Environ. Sci.* **2013**, *6*, 943.
(4) Esposito, D. V.; Hunt, S. T.; Kimmel, Y. C.; Chen, J. G. G. *J. Am. Chem. Soc.* **2012**, *134*, 3025.
(5) Porosoff, M. D.; Yang, X. F.; Boscoboinik, J. A.; Chen, J. G. G. *Angew. Chem., Int. Ed.* **2014**, *53*, 6705.
(6) Zheng, W. Q.; Cotter, T. P.; Kaghazchi, P.; Jacob, T.; Frank, B.; Schlichte, K.; Zhang, W.; Su, D. S.; Schuth, F.; Schlogl, R. *J. Am. Chem. Soc.* **2013**, *135*, 3458.
(7) Oshikawa, K.; Nagai, M.; Omi, S. *J. Phys. Chem. B* **2001**, *105*, 9124.
(8) Ma, Y. F.; Guan, G. Q.; Phanthong, P.; Hao, X. G.; Huang, W.; Tsutsumi, A.; Kusakabe, K.; Abudula, A. *J. Phys. Chem. C* **2014**, *118*, 9485.
(9) Nagai, M.; Matsuda, K. *J. Catal.* **2006**, *238*, 489.
(10) Shi, C.; Zhang, A. J.; Li, X. S.; Zhang, S. H.; Zhu, A. M.; Ma, Y. F.; Au, C. T. *Appl. Catal., A* **2012**, *431*, 164.
(11) Ji, N.; Zhang, T.; Zheng, M. Y.; Wang, A. Q.; Wang, H.; Wang, X. D.; Chen, J. G. G. *Angew. Chem., Int. Ed.* **2008**, *47*, 8510.
(12) Dong, S. M.; Chen, X.; Zhang, X. Y.; Cui, G. L. *Coord. Chem. Rev.* **2013**, *257*, 1946.
(13) Dong, S. M.; Chen, X.; Zhang, K. J.; Gu, L.; Zhang, L. X.; Zhou, X. H.; Li, L. F.; Liu, Z. H.; Han, P. X.; Xu, H. X.; Yao, J. H.; Zhang, C. J.; Zhang, X. Y.; Shang, C. Q.; Cui, G. L.; Chen, L. Q. *Chem. Commun.* **2011**, *47*, 11291.
(14) Zhang, K. J.; Zhang, L. X.; Chen, X.; He, X.; Wang, X. G.; Dong, S. M.; Han, P. X.; Zhang, C. J.; Wang, S.; Gu, L.; Cui, G. L. *J. Phys. Chem. C* **2013**, *117*, 858.
(15) Chen, W. F.; Sasaki, K.; Ma, C.; Frenkel, A. I.; Marinkovic, N.; Muckerman, J. T.; Zhu, Y. M.; Adzic, R. R. *Angew. Chem., Int. Ed.* **2012**, *51*, 6131.
(16) Wang, S. M.; Yu, X. H.; Lin, Z. J.; Zhang, R. F.; He, D. W.; Qin, J. Q.; Zhu, J. L.; Han, J.; Wang, L.; Mao, H. K.; Zhang, J. Z.; Zhao, Y. S. *Chem. Mater.* **2012**, *24*, 3023.
(17) Schweitzer, N. M.; Schaidle, J. A.; Ezekoye, O. K.; Pan, X. Q.; Linic, S.; Thompson, L. T. *J. Am. Chem. Soc.* **2011**, *133*, 2378.
(18) Calle-Vallejo, F.; Koper, M. T. M.; Bandarenka, A. S. *Chem. Soc. Rev.* **2013**, *42*, 5210.
(19) Koper, M. T. M. *Nat. Chem.* **2013**, *5*, 255.
(20) Schaidle, J. A.; Schweitzer, N. M.; Ajenifujah, O. T.; Thompson, L. T. *J. Catal.* **2012**, *289*, 210.
(21) Liao, L.; Wang, S. N.; Xiao, J. J.; Bian, X. J.; Zhang, Y. H.; Scanlon, M. D.; Hu, X. L.; Tang, Y.; Liu, B. H.; Girault, H. H. *Energy Environ. Sci.* **2014**, *7*, 387.
(22) Zhao, Y.; Watanabe, K.; Hashimoto, K. *J. Am. Chem. Soc.* **2012**, *134*, 19528.
(23) Tian, J. Q.; Liu, Q.; Asiri, A. M.; Sun, X. P. *J. Am. Chem. Soc.* **2014**, *136*, 7587.
(24) Popczun, E. J.; McKone, J. R.; Read, C. G.; Biacchi, A. J.; Wiltrout, A. M.; Lewis, N. S.; Schaak, R. E. *J. Am. Chem. Soc.* **2013**, *135*, 9267.
(25) Jaksic, M. M. *Int. J. Hydrogen Energy* **2001**, *26*, 559.
(26) Danilovic, N.; Subbaraman, R.; Strmcnik, D.; Chang, K. C.; Paulikas, A. P.; Stamenkovic, V. R.; Markovic, N. M. *Angew. Chem., Int. Ed.* **2012**, *51*, 12495.
(27) Xie, J. F.; Zhang, J. J.; Li, S.; Grote, F.; Zhang, X. D.; Zhang, H.; Wang, R. X.; Lei, Y.; Pan, B. C.; Xie, Y. *J. Am. Chem. Soc.* **2013**, *135*, 17881.
(28) Lukowski, M. A.; Daniel, A. S.; Meng, F.; Forticaux, A.; Li, L. S.; Jin, S. *J. Am. Chem. Soc.* **2013**, *135*, 10274.
(29) Cao, B. F.; Veith, G. M.; Neuefeind, J. C.; Adzic, R. R.; Khalifah, P. G. *J. Am. Chem. Soc.* **2013**, *135*, 19186.
(30) Vrubel, H.; Hu, X. L. *Angew. Chem., Int. Ed.* **2012**, *51*, 12703.
(31) Zhu, Y. W.; Yuan, Z. C.; Cui, W.; Wu, Z. W.; Sun, Q. J.; Wang, S. D.; Kang, Z. H.; Sun, B. Q. *J. Mater. Chem. A* **2014**, *2*, 1436.
(32) Horn, J. M.; Song, Z.; Potapenko, D. V.; Hrbek, J.; White, M. G. *J. Phys. Chem. B* **2005**, *109*, 44.

DOI: 10.1021/ja5114529
J. Am. Chem. Soc. 2015, 137, 110−113